Intrinsic fluorescence and redox changes associated with apoptosis of primary human epithelial cells

Jonathan M. Levitt
Tufts University
Biomedical Engineering Department
Medford, Massachusetts 02155

Amy Baldwin
Harvard Medical School
Brigham and Women's Hospital
The Channing Laboratory
Department of Medicine
Boston, Massachusetts 02115

Antonios Papadakis
University Hospital of Herakleion
Radiology Department
Herakleion, Greece 71110

Sameer Puri
Joanna Xylas
Tufts University
Biomedical Engineering Department
Medford, Massachusetts 02155

Karl Münger
Harvard Medical School
Brigham and Women's Hospital
The Channing Laboratory
Department of Medicine
Boston, Massachusetts 02115

Irene Georgakoudi
Tufts University
Biomedical Engineering Department
Medford, Massachusetts 02155
and
Massachusetts General Hospital
Wellman Center for Photomedicine
Boston, Massachusetts 02114
E-mail: Irene.Georgakoudi@tufts.edu

Abstract. Apoptosis plays a key role in the development and maintenance of human tissues. This process has been studied traditionally in cells that are stained with exogenous fluorophores. These approaches affect cell viability, and thus are ill-suited for *in vivo* applications. We present an imaging approach that can identify apoptotic cells in living cell populations based on detection and quantification of distinct changes in the intensity and localization of cellular autofluorescence. Specifically, we acquire NAD(P)H, FAD, and redox ratio autofluorescence images of primary keratinocytes following 1, 9, 14, and 18 h of treatment with cisplatin, a known apoptosis-inducing chemotherapy agent. We find that intense autofluorescence combined with a low redox fluorescence ratio is progressively confined to a gradually smaller perinuclear cytoplasmic region with cisplatin treatment. Studies with exogenous nuclear fluorophores demonstrate that these autofluorescence changes occur at early stages of apoptosis. Additional costaining experiments suggest that this strongly autofluorescent, highly metabolically active perinuclear ring represents a subpopulation of mitochondria that are mobilized in response to the apoptotic stimulus and may provide the energy required to execute the final apoptotic steps. Thus, autofluorescence localization changes could serve as a sensitive, noninvasive indicator of early apoptosis *in vivo*.
 [DOI: 10.1117/1.2401149]

Keywords: fluorescence; apoptosis; optical diagnosis; microscopy; redox ratio.

Paper 06029RR received Feb. 16, 2006; revised manuscript received Jul. 19, 2006; accepted for publication Jul. 19, 2006; published online Dec. 18, 2006.

1 Introduction

Early detection of epithelial cancers, including breast, prostate, colon, cervical, and oral cancer, is a key prognostic factor.[1] However, precancerous and early cancerous lesions are difficult to detect by current noninvasive modalities such as endoscopy, colposcopy, colonoscopy, and even by biopsy. Therefore, the development of novel, sensitive methods that allow clinicians to distinguish diseased from healthy tissues promises to have a significant impact on early detection of precancerous lesions, and consequently, the management of cancer patients. One such approach involves identification of unique, endogenous optical cellular signatures based on fluorescence, light scattering, or Raman signals that can serve as hallmarks of early cancer.[2] Major advantages of such methods include their noninvasive nature, the capability to provide results in real time, as well as the potential for high sensitivity and specificity.

A number of clinical studies have been performed that have demonstrated the potential of optical spectroscopic and imaging techniques for the early detection of cervical,[3–7] lung,[8] esophageal,[9–11] bladder,[12] and breast cancer.[13,14] Fluorescence signals from tryptophan, NADH, FAD, collagen, elastin, and/or porphyrins are often used as biomarkers for

Address all correspondence to Irene Georgakoudi, Biomedical Engineering, Tufts University, 4 Colby St., Rm. 153, Medford, MA 02155; Tel: 617–627–4353; Fax: 617–627–3231; E-mail: Irene.Georgakoudi@tufts.edu

1083-3668/2006/11(6)/064012/10/$22.00 © 2006 SPIE

changes in protein expression, metabolic activity, structural protein integrity, and heme biosynthesis, which are in turn associated with the onset of cancer. The goal of our study is to identify changes in tissue autofluorescence that are associated with specific processes that are known to be subverted during initiation and progression of cancer.[15]

One such process is apoptosis or programmed cell death. Apoptosis is a tumor suppressive pathway and many cells that acquire oncogenic alterations are initially removed by p53-dependent apoptosis.[16] Hence, early neoplastic lesions may exhibit higher rates of apoptosis than surrounding normal tissue. Apoptosis also plays a significant role in tumor cell death in response to chemo- and radiation therapies.[17]

Apoptosis involves a well-orchestrated series of events, with mitochondria and the nucleus as the main regulators. Mitochondria are excellent optical targets because they often exhibit strong autofluorescence associated with two coenzymes involved in oxidative phosphorylation, namely NADH and FAD. Changes in the fluorescence intensity of these chromophores in response to different apoptotic stimuli have been previously reported, based primarily on spectroscopic and flow cytometric measurements.[18–22] In addition, a small number of fluorescence imaging studies have indicated that diffuse relocalization of NADH autofluorescence from the mitochondria to the entire cytoplasm occurs at the early apoptotic stages.[19,23]

The goal of this study was to examine, in a quantitative way, distinct changes in the *localization and intensity* patterns of subcellular NADH and FAD fluorescence associated with apoptosis in primary human epithelial cells. In addition, we sought to understand such changes in the context of subcellular metabolic activity by examining the corresponding fluorescence redox ratio images. The redox ratio, defined as the ratio of [FAD] to [NADH+FAD], has been used effectively as an indicator of metabolic activity.[18,24–26] This parameter yields more reliable information than either NADH or FAD fluorescence alone, because it is less susceptible to instrumentation parameters and attenuation by hemoglobin absorption. Thus, it could serve as a suitable quantitative parameter for extending the present studies to *in-vivo* diagnostic applications. Since NADH and its phosphorylated form, NADPH, found typically throughout the cytoplasm, have identical fluorescence excitation and emission spectra, we have used the notation NAD(P)H throughout the work to indicate that the observed fluorescence could be attributed to both molecules. However, it is known that both the quantum efficiency and cellular concentration of NADH is significantly higher than that of NADPH.[27,28] Thus, we expect that our findings reflect predominantly changes in NADH, which is the more relevant metabolic reporter.

2 Materials and Methods

2.1 *Cell Culture*

Primary human foreskin keratinocytes (HFKs) were obtained from neonatal foreskins and cultured as described elsewhere.[29] Cells were grown in keratinocyte serum-free media supplemented with epidermal growth factor, bovine pituitary extract (KSFM, Invitrogen, Carlsbad, California), containing 0.1% gentamicin, 0.2% fungizone, and 1% penicillin-streptomycin in 100×200-mm tissue culture dishes (Falcon, Franklin Lakes, New Jersey). HFKs were passaged 1:5 once per week when 80% confluence was reached for up to four weeks (passage 5). For fluorescent measurements, cells were plated on #1.5, 25-mm glass cover slips at a density of 350,000 cells the day prior to cisplatin treatment. Cells were maintained in a 37 °C, 5% CO_2 incubator.

2.2 *Apoptosis Treatment and Imaging*

To induce apoptosis, HFKs grown on glass coverslips were treated with 10 μg/ml of cisplatin (cis-diamminedichloroplatinum, Sigma, Saint Louis, Missouri; 10-mg/ml stock in dimethyl sulfoxide-DMSO) in KSFM. Control cells were treated with solvent (DMSO) at a concentration of 1:1000 by volume in media. After 1, 9, 14, and 18 h of treatment, coverslips were removed from the incubator and placed in an attofluor cell chamber (Molecular Probes, Carlsbad, California) with 1.5 ml of standard media diluted with phosphate-buffered saline at a ratio of 1:1.

An Olympus BX-51 upright microscope with a 40×, 0.8 numerical aperture objective (Olympus, Melville, New York) was used to detect cellular autofluorescence. For NAD(P)H fluorescence excitation and emission, we used a filter set including a 365/20-nm bandpass exciter (Omega, Brattleboro, Vermont), a 380 DCLP dichroic (Chroma, Rockingham, Vermont), and a 450/65-nm bandpass emitter (Omega). For FAD imaging, we used a filter set including a 455/40-nm bandpass exciter (Omega), a 460 DCLP dichroic (Chroma), and a 520/40-nm emitter (Omega). Intensity images were captured using a SPOT RT Slider 2 megapixel 12-bit camera in monochrome mode (Diagnostic Instruments, Sterling Heights, Michigan). The image acquisition time was typically 3 s for NAD(P)H imaging and 4 s for FAD imaging. Three to six fields were imaged from each coverslip and at least two coverslips per time point were examined for each experiment.

2.3 *Cell Staining Protocols*

To assess the effects of cisplatin treatment on mitochondrial membrane depolarization and nuclear morphology, we performed costaining with 500-nM MitoTracker Orange (Molecular Probes) and 10 μg/ml Hoechst 33342 (Sigma), respectively. MitoTracker fluorescence was detected using a filter set containing a 540/25-nm bandpass exciter (Olympus), 565 DCLP nm dichroic (Chroma), and 580-nm longpass emitter (BA580IF, Olympus). The filter set used for FAD imaging was also used to observe Hoechst fluorescence. A stage holder that allowed removal of the attofluor chamber from the microscope stage, cell staining, and accurate repositioning for acquisition of colocalized NAD(P)H/FAD and MitoTracker/Hoechst images was designed and built in-house. Hoechst and MitoTracker imaging required very short acquisition times (50 ms) compared to the times required for NAD(P)H and FAD imaging (3 and 4 s, respectively). Thus, it was possible to acquire autofluorescence images, stain the cells, and then acquire the corresponding MitoTracker and Hoechst images without any significant crosstalk.

To assess the potential role of translocation of apoptosis inducing factor (AIF) from mitochondria to the nucleus in the autofluorescence localization changes that are induced by cisplatin treatment, we performed AIF-antibody staining. Briefly, cells were fixed with a 10% formalin solution, permeabilized

with a 2% TritonX solution, and incubated with normal sheep serum (013-000-121, Jackson Immunoresearch, West Grove, Pennsylvania) for 20 min to minimize nonspecific binding. Next, approximately 500,000 cells were treated for 1 h with a 1:50 dilution of primary rabbit anti-AIF antibody (2267; QED Bioscence Incorporated, San Diego, California), and then for 45 min with a 1:500 dilution of secondary goat-anti-rabbit IgG (STAR35A; Serotec, Kidlington, United Kingdom) conjugated to R. phycoerythrine (RPE). Control experiments were performed without the primary antibody confirming only nonspecific staining. To visualize RPE fluorescence, we used the MitoTracker Orange filter set.

2.4 *Image Processing*

Using established protocols, NAD(P)H and FAD calibration curves were created to allow association between fluorescence intensity and molar concentration.[30] NAD(P)H and FAD fluorescence intensity images were then weighted such that the pixel values in a given image corresponded to the concentration of the fluorophore. Thus, redox ratios could be determined accurately.

To quantify the changes in the localization patterns of NAD(P)H and FAD fluorescence in response to cisplatin treatment, we developed analysis software based on the MATLAB platform (Mathworks, Natick, Massachusetts). The image analysis program hierarchy consists of three major components: cell selection, fluorescence intensity extraction, and data processing. Each of these processes can be run independently or in concert.

The cell selection portion of the program identifies and gathers all cytoplasmic NAD(P)H and FAD images for all time points and treatments for a given experiment. For a particular field, the user is shown a redox intensity image [FAD]/{[NAD(P)H]+[FAD]} and then zooms to a particular cell location to select the outer cell border. The user then outlines the nuclear border based on a FAD image stretched to the full grayscale dynamic range [Fig. 1(a)]. The cell selection program cycles through all cells in each field for every time point of the experiment and stores the coordinates of each outer cell and corresponding nuclear border the user has identified. For each experiment, we processed on average 250 cells per treatment, per time point, and our data represents collectively measurements from 6044 cells. A small number of fibroblasts, binucleated, or noncoplanar cells present in the fields examined were excluded from analysis.

In the fluorescence intensity extraction element of the program, each cell is independently analyzed to compute the intense perinuclear cytoplasmic fluorescent area and the mean pixel intensity. The cell image is converted to a polar intensity plot of angle versus distance from the center of the nucleus [Figure 1(c)] and then normalized to the distance from the nuclear border [Figs. 1(d) and 1(e)]. Fluorescence plots are divided into 36 sections and the intensity of each 10-deg section is averaged along the horizontal direction to reduce noise. By using a combination of generic first- and second-derivative edge detection algorithms provided by the Matlab software, the border of the fluorescent region is determined for each section [Fig. 1(e)]. For each cell, the area and the mean fluorescence intensity per pixel is computed for the entire cytoplasm and the intense fluorescent perinuclear ring.

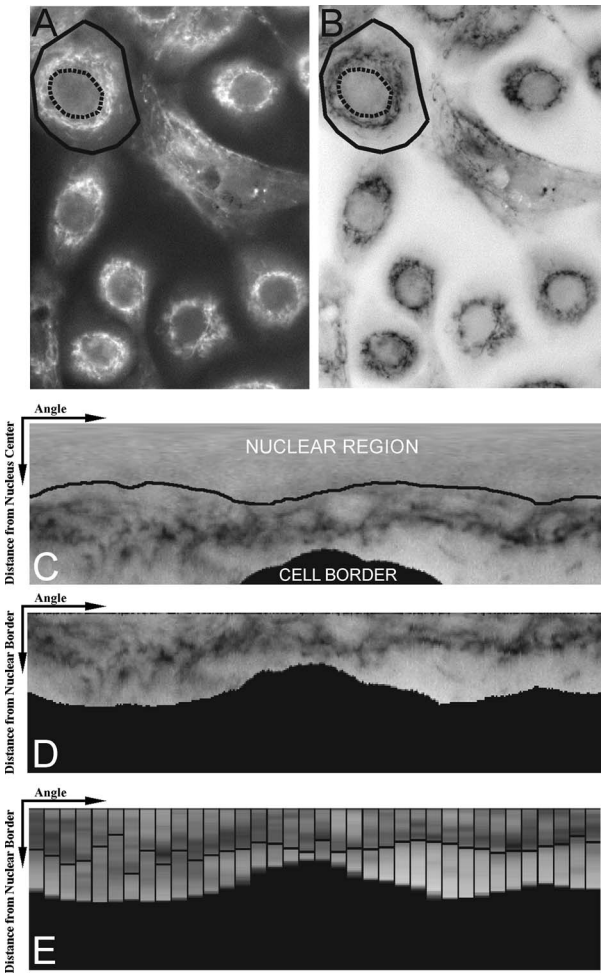

Fig. 1 Stages of quantitative image analysis. Redox ratio images of the same field using (a) an inverted and (b) a standard (i.e., lowest intensity=black; highest intensity=white) grayscale map. The cell and nuclear border of one of the cells are indicated with a solid and dashed line, respectively. (c) Cell image converted to polar coordinates; the solid line represents the nuclear border. The *x* axis represents polar angle and the *y* axis distance from the nucleus center. (d) Corresponding image of the cytoplasmic fluorescence only (i.e., nuclear border set to 0 on *y* axis) (e) Cytoplasmic fluorescence following intensity averaging over 10 deg in the horizontal direction and edge detection; edge indicated with horizontal solid line in each 10° segment.

Finally, in the data processing component of the program, all the cellular area and mean pixel intensity data for each time point and experiment are grouped and displayed for visual inspection.

2.4.1 *Statistical analysis*

A standard two-tailed Student's t-test was used to assess differences in the means at a significance level of $p < 0.05$. Standard errors of the mean intensity were calculated based on the means, standard deviations, and corresponding number of cells for each experiment, time point, and treatment group. These errors were propagated to calculate the standard errors of the means of the values of NAD(P)H, FAD, and redox ratio intensities of the cisplatin-treated cells when normalized to the corresponding values of the control (DMSO-treated)

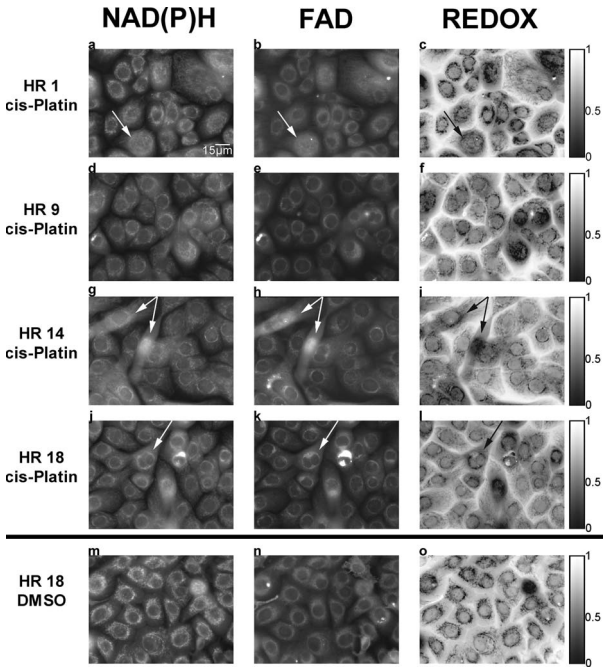

Fig. 2 NAD(P)H, FAD, and calculated redox ratio fluorescence images of cells treated either with cisplatin for (a), (b), and (c) 1 h, (d), (e), and (f) 9 h, (g), (h), and (i) 14 h, and, (j), (k), and (l), 18 h or with DMSO [vehicle control, (m), (n), and (o)] for 18 h. Arrows indicate the types of cells that were excluded from quantitative image analysis, such as (a), (b), and (c), cells lifting off the coverslip, (g), (h), and (i) fibroblasts, and (j), (k), and (i) binucleated cells. The image intensities are stretched to enhance visualization of localized features.

cells.[31] A 2×2 exponential analysis of variance (ANOVA) test was performed to assess statistical differences between the DMSO- and cisplatin-treated cells when considering a combination of the redox ratio and the extent of the strongly fluorescent perinuclear ring, i.e., data included in Fig. 3.[32]

3 Results

To identify intrinsic hallmarks associated with apoptosis, we acquired NAD(P)H and FAD intensity images of primary human foreskin keratinocytes (HFKs) treated with cisplatin, an established apoptosis-inducing chemotherapy agent. We generated corresponding redox images, and compared the NAD(P)H, FAD, and redox fluorescence ratio intensities measured at 1, 9, 14, and 18 h after the onset of cisplatin treatment. After one hour of treatment, both NAD(P)H and FAD fluorescence is observed throughout a significant portion of the cytoplasm [Figs. 2(a)–2(c): arrows point to cells excluded from quantitative analysis as discussed later]. However, as early as 9 h after the onset of treatment, there are noticeable changes in the autoflourescence patterns of cisplatin-treated cells, and a well-defined ring-like structure surrounding the nucleus is detected [Figs. 2(d)–2(f)]. This confined, strongly autofluorescent ring is present even more prominently after 14 h [Figs. 2(g)–2(i)] and 18 h [Figs. 2(j)–2(l)] of treatment. In contrast, cells treated with solvent (DMSO) for up to 18 h continue to exhibit strong fluorescence throughout a significant portion of the cytoplasm [Figs. 2(m)–2(o)]. Thus, the appearance of the confined perinuclear autofluorescence ring is a specific response to cisplatin treatment.

To quantify and assess the reproducibility of the fluorescence changes that we attribute to cisplatin treatment, we developed algorithms that identify and display the area and mean pixel intensity of the fluorescence within the entire cytoplasm and the intensely fluorescing perinuclear area. To ensure reliable results, small numbers of nonkeratinocytes and cells undergoing morphological changes independent of drug treatments were excluded, as indicated by the arrows in Fig. 2. Specifically, we eliminated from this analysis cells that did not possess a dark-nuclear region [Figs. 2(a)–2(c)] or were lifting off the coverslip, either because they were preparing for mitosis or dying. We also excluded fibroblasts, which are invariably present at low numbers in our cultures [Figs. 2(g)–2(i)] and binucleated cells [Figs. 2(j)–2(l)].

In Fig. 3, we show an example of the quantitative information acquired from a representative experiment. Specifically, Fig. 3 displays the values of the mean redox ratio of the strongly fluorescent perinuclear ring as a function of the ring area normalized to the nuclear area for every one of the cells analyzed at each treatment time point. The normalized perinuclear ring area accounts for variations in nuclear size and represents more accurately the ring thickness, which in turn is the parameter that clearly changes with the progression of apoptosis, as seen in Fig. 2. At 1 h following treatment, the thickness and the redox ratio of the strongly fluorescent perinuclear ring is very similar (i.e., no statistical difference for $p<0.05$) for the DMSO (control)- and cisplatin-treated groups [Fig. 3(a)]. However, within 9 h of treatment, we observe that the distribution of values corresponding to the cisplatin-treated cells is shifted significantly to lower redox ratios compared to the DMSO-treated cells [Fig. 3(b)]. By 14 h there is also a clear shift toward more localized (thinner) fluorescent perinuclear rings for the cells that are undergoing apoptosis compared to the control population of keratinocytes [Fig. 3(c)]. This trend persists at 18 h following the onset of treatment, even though we see a greater level of overlap in the redox ratio intensity of the DMSO- and cisplatin-treated cells, than at 9 and 14 h. The differences observed in the two populations at 9, 14, and 18 h are statistically significant based on a 2×2 exponential ANOVA test ($p<0.05$).

Similar changes have been observed in three independent experiments and a summary of the quantitative image analysis results are presented in Fig. 4. Figure 4(a) illustrates that the extent of the intensely fluorescent/low redox ratio perinuclear area becomes gradually smaller in the cisplatin group compared to the control group, with the differences reaching statistical significance at the 9-h treatment time point and remaining significant at 14 and 18 h of treatment ($p<0.05$) [Fig. 4(a)]. To assess the presence of intensity differences, we first calculated the mean pixel intensity per cell for NAD(P)H, FAD, and the redox ratio for the entire cytoplasm and the strongly fluorescent perinuclear ring. We used these values to estimate the mean intensity of each parameter [i.e., NAD(P)H, FAD, and redox ratio] for each time point and treatment group (i.e., control and cisplatin). To ensure that any differences that we detect are attributed to cisplatin treatment alone, we normalized at every time point the mean value of each parameter [i.e., NAD(P)H, FAD, and redox ratio] representing the

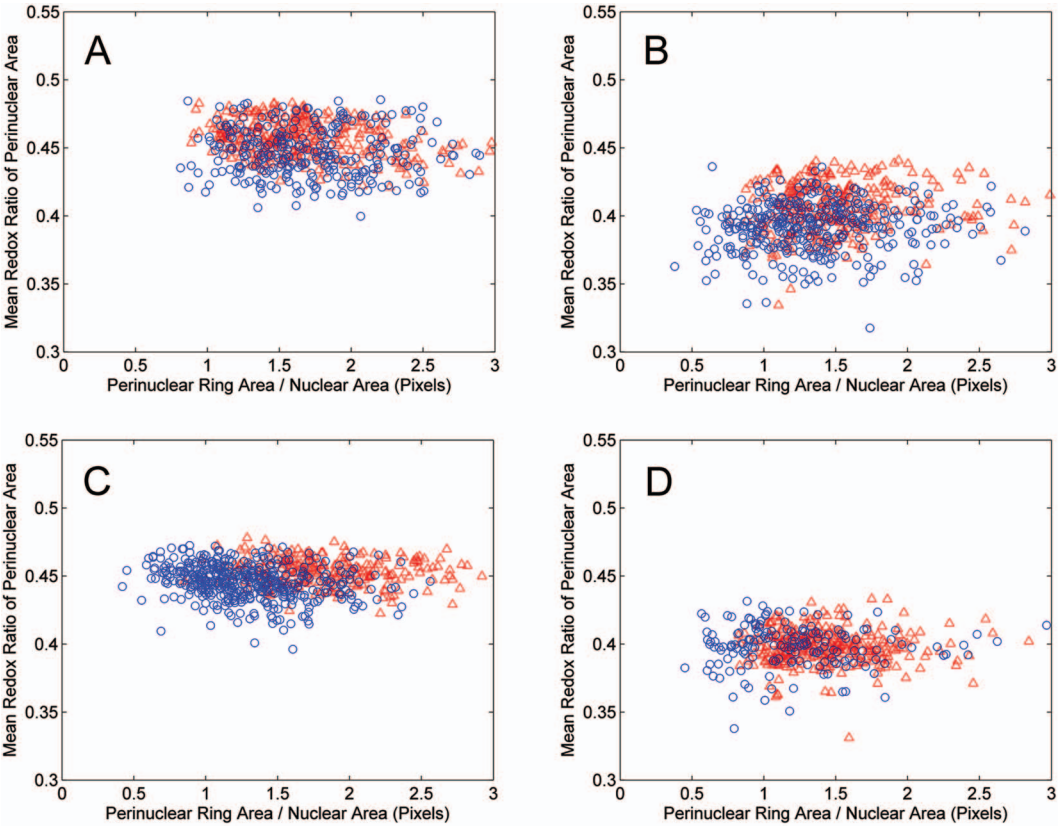

Fig. 3 The mean fluorescence redox ratio per cell is plotted as a function of the perinuclear ring area normalized to the nuclear area for each cell of a representative experiment. Cells were treated either with cisplatin (blue circles, apoptosis group) or DMSO (red triangles, control) for (a) 1, (b) 9, (c) 14, and (d) 18 h. The two cell populations overlap initially (1 h), indicating similar redox intensity and ring thickness values for the two groups. However, they become statistically distinct as early as 9 h of treatment, with the cisplatin cells exhibiting a significant decrease in the extent of the perinuclear ring and its redox ratio [(b), (c), and (d)].

cisplatin-treated cells to the corresponding mean value for the DMSO-treated cells. We observe an initial increase in NAD(P)H fluorescence at the 9-h treatment time point that is followed by a decrease to the levels of the control population by 14 h of treatment [Figs. 4(b) and 4(c)]. The changes in NAD(P)H fluorescence are similar independent of whether we are considering the entire cytoplasm or the localized perinuclear ring, with the mean intensity at 9 h statistically different from that at 1, 14, and 18 h of treatment ($p<0.05$). The cytoplasmic FAD fluorescence intensity follows the same pattern of changes as NAD(P)H fluorescence. However, within the perinuclear ring we observe an increase in FAD intensity for the 9- and 14-h treatment points that is statistically different from the 1- and 18-h intensities ($p<0.05$). Interestingly, the changes that we observe when we consider the redox ratio are different both in the case of the cytoplasmic and perinuclear ring areas. Specifically, we find that the redox ratio of the entire cytoplasm decreases significantly after 9 h of cisplatin treatment ($p<0.05$), but gradually increases as treatment progresses (all means are statistically different at $p<0.05$, with the exception of the 1- and 14-h time points). The redox ratio intensity corresponding to the strongly fluorescent perinuclear ring also decreases significantly ($p<0.05$) at 9 h of treatment, and remains lower than the 1-hour time point following 14 (statistically different for $p<0.05$) and 18 h of treatment (statistically different for $p<0.10$). Since the redox ratio intensity is inversely related to metabolic activity, the significant changes we observe at 9 and 14 h suggest that the rate of energy production is enhanced in response to cisplatin treatment in the area immediately surrounding the nucleus compared to the rest of the cytoplasm.

To ensure that cisplatin treatment did indeed induce changes in nuclear morphology that are characteristic of apoptosis, we performed Hoechst DNA staining experiments. At 1 h of cisplatin treatment and at 18 h of DMSO-treatment, we observe uniform nuclear Hoechst staining, as expected for normal cells (Fig. 5). However, as early as 9 h after the onset of cisplatin treatment, we observe more punctuate Hoechst nuclear staining and irregularities in the nuclear perimeter, consistent with the characteristic morphological nuclear changes of apoptosis. Representative Hoechst fluorescence images of cells treated for 1, 9, 14, and 18 h with cisplatin or for 18 h with solvent (DMSO) are shown in Fig. 5.

To confirm that the formation of a confined perinuclear fluorescence ring occurs during earlier rather than later stages of apoptosis, we designed an insert for the microscope stage that allowed us to acquire NAD(P)H/FAD and Hoechst images of the same fields. A representative example is shown in Fig. 6 for HFKs that have been treated with cisplatin for 24 h. Cells with structurally intact (i.e., unfragmented) nuclei exhibit a strong perinuclear autofluorescence ring. Conversely, the late stage apoptotic cells with distinctly fragmented

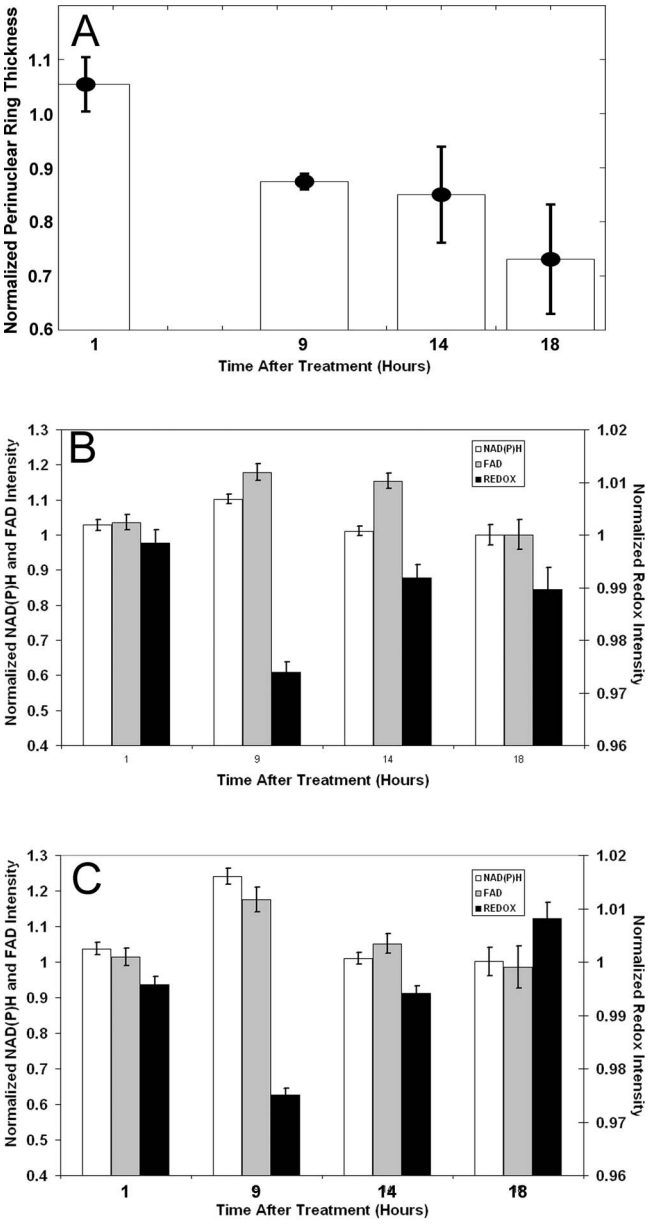

Fig. 4 Mean and standard error of the fluorescence perinuclear ring thickness and intensity per pixel for cisplatin-treated cells normalized to the values of the corresponding DMSO-treated populations from three independent experiments. (a) The extent of the strongly fluorescent perinuclear ring becomes gradually smaller for cisplatin-treated cells compared to DMSO-treated cells as treatment progresses. (b) Within the strongly fluorescent perinuclear area, there is an initial increase in the NAD(P)H (white bars) and FAD (gray bars) fluorescence following 9 h of cisplatin treatment that is followed by a decrease as treatment progresses. The corresponding redox ratio intensity (black bars) decreases at 9 h and remains statistically lower at 14 ($p<0.05$) or 18 h ($p<0.10$) of treatment compared to 1 h. (c) The overall cytoplasmic NAD(P)H (white bars) and FAD (gray bars) fluorescence intensities increase at 9 h and decrease for longer treatments. The fluorescence redox ratio intensity of the entire cytoplasm (black bars) also decreases significantly at 9 h of cisplatin treatment. However, in contrast to the redox ratio of the perinuclear area, the cytoplasmic redox ratio increases significantly at 14 h and continues to increase as treatment progresses. For (b) and (c) the intensity scale on the left is for normalized NAD(P)H and FAD fluorescence, while the scale on the right is for the normalized redox ratio.

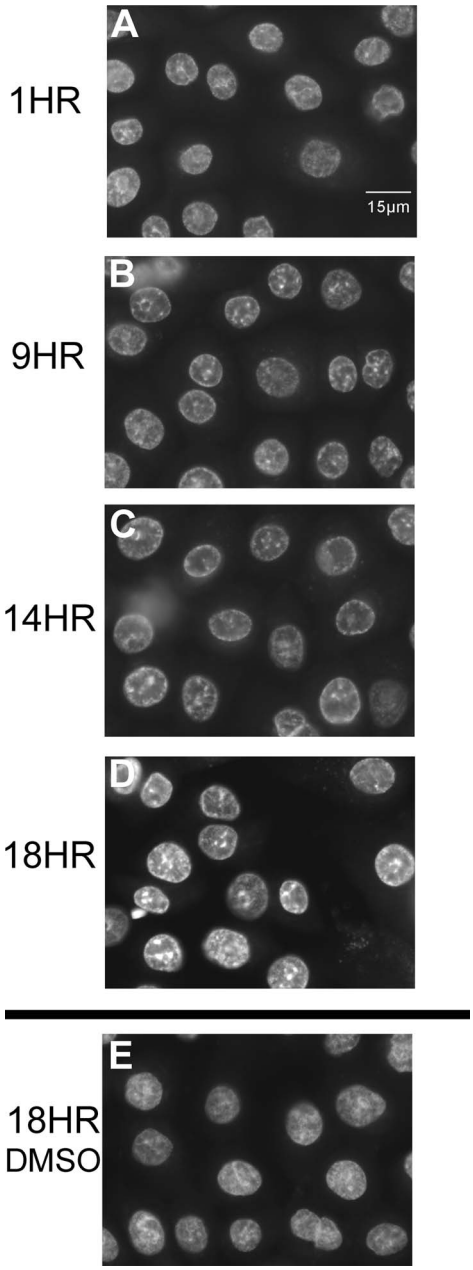

Fig. 5 Representative fluorescence images of cells whose nuclei have been stained with Hoechst following either 1, 9, 14, or 18 h of cisplatin treatment [(a)] through (d), respectively] or (e) 18 h of DMSO treatment. More punctate nuclear staining is present as early as 9 h following the onset of cisplatin treatment, while no significant changes are observed even after 18 h of DMSO treatment (control group).

Hoechst-stained nuclei display low intensity, diffusely localized autofluorescence. Thus, formation of the strongly fluorescent/low redox ratio perinuclear ring preceeds nuclear fragmentation and occurs at an earlier stage of apoptosis.

Since disruption of mitochondrial transmembrane potential is a key early hallmark of many forms of apoptosis, we sought to determine whether the observed autofluorescence changes can be correlated to changes in mitochondrial membrane integrity as reported by MitoTracker Orange fluorescence. Mi-

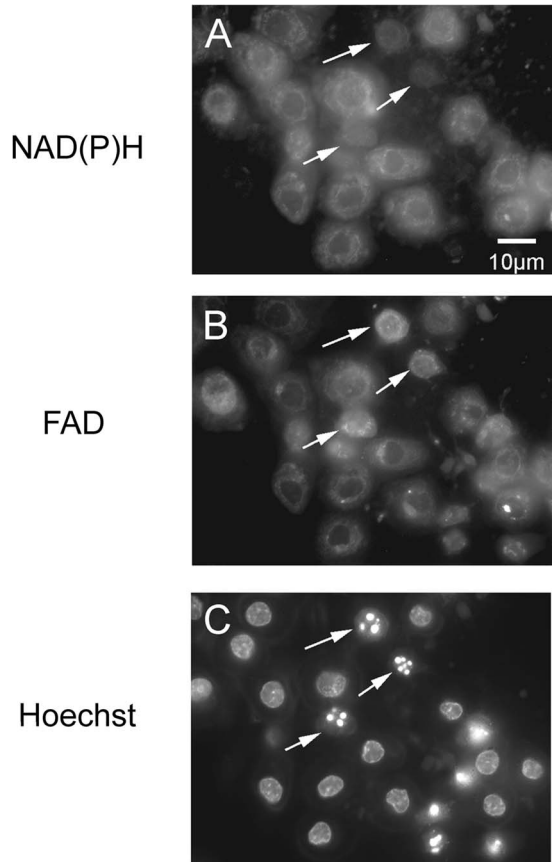

Fig. 6 (a) NAD(P)H, (b) FAD, and (c) Hoechst flourescence images of the same field after 24 h of cisplatin treatment. Cells with fragmented nuclei indicated by arrows have very low and/or diffuse autofluorescence and do not exhibit an intense perinuclear fluorescence ring.

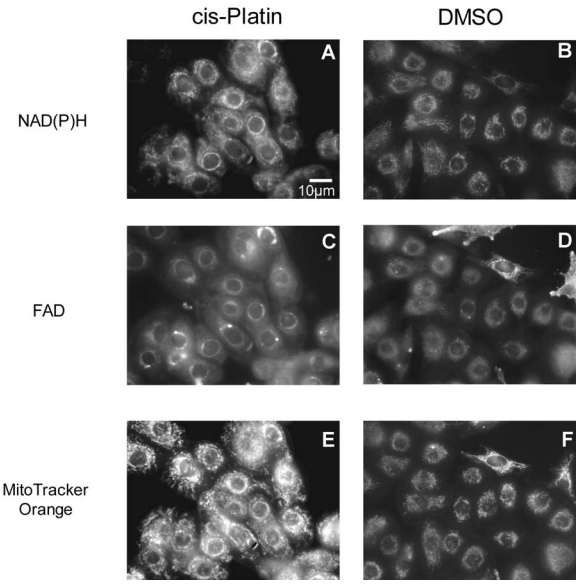

Fig. 7 (a) and (b) NAD(P)H, (c) and (d) FAD, and (e) and (f) MitoTracker flourescence images of the same field after 18 h of, (a), (c), and (e) cisPlatin or (b), (d), and (f) DMSO treatment. The corresponding patterns of NAD(P)H and FAD autofluorescence are very similar to the patterns acquired after MitoTracker staining, indicating that the strongly autofluorescent perinuclear area represents metabolically active mitochondria. All image intensities are stretched to the full dynamic range of the camera to enhance visualization of localized features.

toTracker Orange, a cell permeable compound, is actively transported into intact mitochondria where it is oxidized and becomes fluorescent. Colocalized images of endogenous and MitoTracker fluorescence confirm that NAD(P)H and FAD fluorescence emanates from intact mitochondria that form punctate or tubular networks throughout the cytoplasm of normal (DMSO-treated) cells [Figs. 7(b), 7(d), and 7(f)]. Upon cisplatin treatment, distinct perinuclear MitoTracker fluorescent rings are detected, similar to the corresponding NAD(P)H and FAD fluorescence [Figs. 7(a), 7(c), and 7(e)]. Thus, the alterations that we observe in the subcellular autofluorescence patterns during early apoptotic stages represent changes in the spatial subcellular organization of active mitochondria.

Another potential contributor to the autofluorescence localization changes that we observe may be associated with the apoptosis inducing factor (AIF). AIF is a protein that is normally contained in the intermembrane space of the mitochondria and it can act both as an electron transferase and an effector of apoptosis.[33–35] It contains binding domains for both NADH and FAD[33,35] and it has been found to translocate from mitochondria to the nucleus, where it is involved in chromatin condensation and high molecular weight DNA fragmentation.[34,36,37] AIF-antibody staining of HFKs treated with DMSO for 14 h indicates that AIF is localized uniformly throughout the cytoplasm [Fig. 8(a)]. However, a significant fraction of cells treated with cisplatin for 14 h exhibits a stronger staining pattern in the perinuclear area. This may be the result of changes in mitochondrial activation patterns, but it may also reflect translocation of AIF toward the nucleus in response to apoptotic stimuli.

4 Discussion

In this study, we demonstrate that the intensity *and* the localization patterns of cellular NAD(P)H, FAD, and the corresponding redox ratio change in response to cisplatin-induced

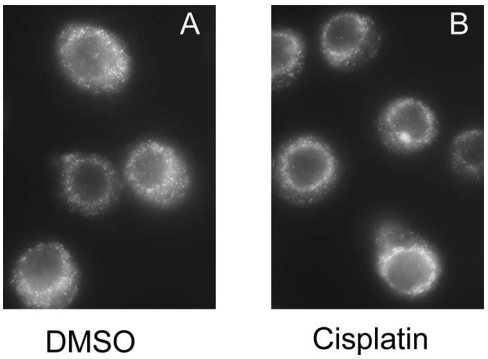

Fig. 8 AIF antibody staining of cells after 14 h of (a) DMSO or (b) cisplatin treatment. While AIF is observed throughout the cytoplasm of cells treated with DMSO, it is confined to the nuclear perimeter in cisplatin-treated cells, similar to the localization of NAD(P)H and FAD autofluorescence.

apoptosis of primary human foreskin keratinocyes (HFKs). Changes in the redox ratio *intensity* are more persistent than changes in NAD(P)H or FAD alone, but unless time-dependent changes are monitored, it would be difficult to use them as specific indicators of apoptosis. However, the autofluorescence *localization* changes we report are prominent and consistent for early apoptotic cells that have not undergone nuclear fragmentation. Thus, with spectroscopic imaging it may be possible to monitor apoptosis *in vivo* without the need for exogenous stains. Specifically, we find that whereas normal HFKs exhibit characteristic mitochondrial autofluorescence distributed in punctate or tubular networks throughout their cytoplasm, apoptotic HFKs exhibit more diffuse cytoplasmic autofluorescence and a confined, high autofluorescence/low redox ratio area extending only a few microns beyond the nuclear membrane (Fig. 2). This strongly fluorescent perinuclear ring is detected prior to nuclear fragmentation as determined by colocalization experiments of autofluorescence and Hoechst nuclear staining (Fig. 6). While previous microscopic studies have reported diffuse relocalization of NAD(P)H and FAD autofluorescence in response to apoptosis induction,[23,19] to our knowledge, this is the first time that a characteristic perinuclearly confined autofluorescence pattern is reported as an early apoptotic marker. Furthermore, we are unaware of any published studies where *cellular* redox ratio images are directly represented as grayscale intensity images, with dark areas representing low redox ratios and high metabolic activity/rapid ATP production. It is interesting to note that these images appear to exhibit a finer level of features than the corresponding NAD(P)H and FAD images. Moreover, the redox ratio images clearly illustrate that mitochondrial energy production at the early apoptotic stages becomes confined to the cellular area surrounding the nucleus.

In addition to the fluorescence localization changes that we observe in response to cisplatin-induced apoptosis, we also report quantitative intensity changes in NAD(P)H, FAD, and redox ratio fluorescence within the entire cytoplasm and the intensely fluorescing perinuclear area. Specifically, we find that the fluorescence of both NAD(P)H and FAD initially increases and then decreases prior to nuclear fragmentation. These results are in agreement with previous flow cytometric studies, which examined NAD(P)H fluorescence changes of human lymphoid B cells in response to campothecin-induced apoptosis[21] and flavin fluorescence of leukemic HL60 cells following camptothecin, TNF-α or γ-irradiation treatment.[22] However, some investigators report either only an increase or a decrease in fluorescence intensity. For example, Petit et al. observed flow cytometrically a decrease in overall NAD(P)H autofluorescence at the early stages of apoptosis induced by αCD95 treatment in Jurkat T cells.[20] Conversely, only an increase in both NAD(P)H and FAD fluorescence intensity was detected following simulated hypogravity-induced apoptosis of cultured endothelial cells.[19] It is possible that the time points at which measurements were made limited observation of the initial increase in the former case and the ensuing decrease in the latter. Alternatively, distinct apoptotic pathways may involve different dynamic fluorescent changes. Nevertheless, an increase in both NAD(P)H and FAD fluorescence, followed by a gradual decrease prior to nuclear fragmentation is consistent with the majority of apoptotic studies and is independent of the cell type or apoptotic stimulus.

While we observe very similar trends in the dynamic changes that take place in NAD(P)H and FAD fluorescence for the entire cytoplasm and the strongly fluorescent perinuclear area, that is not the case for the redox ratio intensity. In particular, we find that the redox ratio intensity of the entire cytoplamic area exhibits dynamics that are exactly opposite to that of the individual chromophores, i.e., an initial decrease followed by a gradual increase. In contrast, the redox ratio intensity of the perinuclear ring area decreases and remains lower than the 1-h treatment value. This finding supports the hypothesis that this strongly fluorescent/low redox ratio perinuclear area represents a distinct population of mitochondria that remain intact and provide the energy required to execute the final apoptotic stages that involve nuclear fragmentation. The hypothesis that the appearance of this localized fluorescence ring is driven by cellular metabolic requirements is further supported by observations of high NAD(P)H/FAD fluorescence and low redox ratio intensities at the metabolically active edge of 9L rat glioma tumors compared to the more metabolically quiescent tumor center.[25] High NAD(P)H and FAD levels in combination with a low redox ratio are also found in rapid ATP production areas of the brain with high oxygen and glucose consumption such as the striatum.[24]

A limited number of studies have examined cellular redox ratio fluorescence changes in response to apoptosis. An increase in the fluorescence redox ratio has been observed spectroscopically in correlation with apoptosis induced by N-(-hydroxyphenyl)retinamide (4-HPR) treatment of normal and simian virus-40 immortalized ovarian epithelial cells.[18] An increasing, but not statistically significant, redox ratio trend was also observed *in vivo* in response to 4-HPR treatment of female adult rhesus macaques.[18] These results are consistent with the increasing trend that we observe in the redox ratio intensity of the entire cytoplasm for the 9-, 14-, and 18-h cisplatin treatment time points. It is possible that the initial decrease was not observed because it occurs earlier than the initial time point at which measurements were acquired by Brewer et al.[18] Spectroscopic imaging studies performed with control and simulated hypogravity-exposed apoptotic cells resulted in very similar or increased values for the ratio of FAD to bound or unbound NAD(P)H, respectively.[19] The apoptotic cells that Morbidelli et al.[19] examined exhibited some late stage apoptotic features, such as cell shrinkage and convolution of the nuclear border. Thus, their results are in agreement with the trends we observe between the control and long treatment time point (e.g., 18 h) cell populations of our study.

The changes in autofluorescence patterns we observe in apoptotic HFKs are consistent with mitochondrial membrane depolarization induced in peripheral cell mitochondria and activation of a perinuclear mitochondrial population (Fig. 7). Dissipation of the mitochondrial membrane potential has been previously linked to changes in the NAD(P)H intensity[20] and localization[23] at early apoptotic stages. However, such changes were not associated with the presence of distinct mitochondrial populations involved in the apoptotic process. Such populations have been reported by D'Herde et al.[38] in the context of a combination of biochemical assays to localize cytochrome c and morphological light and electron microscopy studies. They found that subsets of dysfunctional and functional mitochondria were present in the cell until the final

stages of apoptosis. Morphologically distinct peripheral and perinuclear mitochondrial populations have also been reported for different types of nonapoptotic cells. For example, the peripheral mitochondria of immortalized (HeLa, PAEC, COS-7, and HUVEC) and primary cell lines (hepatocytes, neuronal, and cortical cells) exhibit a higher mitochondrial transmembrane potential than the ones located in the perinuclear area.[39] Heterogeneous mitochondrial populations have also been reported based on depth-resolved NAD(P)H (two-photon) and FAD (confocal) fluorescence imaging of different cell populations, including hepatocytes, cardiomyocytes, and cultured carcinoma cells.[40] In that case, some of the observations were based on confocal imaging at excitation/emission wavelengths consistent with flavin fluorescence. However, it is likely that the very bright punctate fluorescence that is observed is not due to flavin mitochondrial fluorescence but lipofuscin fluorescence emanating most probably from lysosomes.[41]

Changes in the observed AIF staining patterns in response to cisplatin treatment (Fig. 8) may simply also reflect the changes in mitochondrial activation that are reported by MitoTracker staining. However, they may also represent another possible contributor to the appearance of the strongly autofluorescent perinuclear ring, namely translocation of AIF from mitochondria toward the nucleus.

Fluorescence measurements, such as the ones presented in this study, noninvasively provide information on biochemical changes that are associated with apoptosis. Other optical methods based typically on light scattering can provide complementary information on the cellular morphological changes that are characteristic of apoptosis. For example, Shiffer et al. have observed changes in wide angle light scattering diffraction patterns in dexamethasone-induced apoptosis of mouse thymocytes.[42] They attribute the light scattering changes to cell shrinkage at early stages of apoptosis, preceeding externalization of phosphatidylserine, as verified by annexin-V staining.[42] Optical scattering imaging (OSI) has also been used as a method for quantifying morphological changes in apoptotic cells. In OSI, the ratio of light scattered within wide and narrow angles is used as a sensitive measure of particle size.[32] Boustany et al. used optical scatter imaging (OSI) to detect mitochondrial morphological changes associated with staurosporine-induced apoptosis of immortalized CSM14.1 rat neuronal cells.[43] It was found that the ratio of wide- to narrow-angle scattered light decreased to 75% of its initial value within 60 min of treatment, which was 5 to 6 h prior to phosphatidylserine externalization and 9 to 10 h prior to loss of membrane integrity. Therefore, the combination of information from fluorescence and light scattering measurements may serve as an even more sensitive, noninvasive tool to detect apoptosis.

In summary, this work demonstrates that significant autofluorescence changes take place at the early stages of cisplatin-induced apoptosis of primary human foreskin keratinocytes that are driven by changes in cellular energy requirements. Such changes may be exploited by spectroscopic imaging modalities to detect apoptotic cells *in vivo*, and thus, to enhance our ability to monitor this process and assess its significance in disease development and diagnosis. As the most significant and consistent changes that we observe are localization rather than intensity changes, high-resolution imaging modalities such as confocal or multiphoton microscopy would be required to extend these apoptosis studies to 3-D *in-vitro* or *in-vivo* tissues.

Acknowledgments

The authors gratefully acknowledge financial support of this work by National Institutes of Health (NIH) grant proposal R01 CA097966-01 and helpful discussions with colleagues at the MIT Spectroscopy Laboratory directed by Michael Feld.

References

1. *Cancer Prevention and Early Detection Facts and Figures*, American Cancer Society (2004).
2. I. Georgakoudi, J. Motz, V. Backman, G. Angheloiu, A. Haka, M. G. Müller, R. Dasari, and M. S. Field, "Quantitative characterization of biological tissue using optical spectroscopy," in *Biomedical Photonics Handbook*, T. Vo-Dinh, Ed., p. 1–33, CRC Press, Boca Raton, Fl (2003).
3. S. K. Chang, Y. N. Mirabal, E. N. Atkinson, D. Cox, A. Malpica, M. Follen, and R. Richards-Kortum, "Combined reflectance and fluorescence spectroscopy for *in vivo* detection of cervical pre-cancer," *J. Biomed. Opt.* **10**(2), 024031 (2005).
4. M. Follen et al., "Optical technologies for cervical neoplasia: update of an NCI program project grant," *Clin. Adv. Hematol. Oncol.* **3**(1), 41–53 (2005).
5. I. Georgakoudi, E. E. Sheets, M. G. Muller, V. Backman, C. P. Crumb, K. Badizadegan, R. R. Dasari, and M. S. Feld, "Trimodal spectroscopy for the detection and characterization of cervical precancers in vivo," *Am. J. Obstet. Gynecol.* **186**(3), 374–382 (2002).
6. N. Ramanujam, M. Follen Mitchell, A. Mahadeven , S. Thomsen, A. Malpica, T. Wright, N. Atkinson, and R. Richards-Kortum, "Spectroscopic diagnosis of cervical intraepithelial neoplasia (CIN) *in vivo* using laser-induced fluorescence spectra at multiple excitation wavelengths," *Lasers Surg. Med.* **19**, 63–74 (1996).
7. N. Ramanujam, M. Mitchell, A. Mahadeven , S. Warren , S. Thomsen, E. Silva, and R. Richards-Kortum, "*In vivo* diagnosis of cervical intraepithelial neoplasia using 337-nm-excited laser-induced fluorescence," *Proc. Natl. Acad. Sci. U.S.A.* **91**, 10193–10197 (1994).
8. S. Lam et al., "Localization of bronchial intraepithelial neoplastic lesions by fluorescence bronchoscopy," *Chest* **113**, 696–702 (1998).
9. I. Georgakoudi et al., "Fluorescence, reflectance and light scattering spectroscopy for evaluating dysplasia in patients with Barrett's esophagus," *Gastroenterology* **120**, 1620–1629 (2001).
10. M. Panjehpour, B. Overholt, T. Vo-Dinh, R. Haggit, D. Edwards, and F. Buckley, "Endoscopic fluorescence detection of high-grade dysplasia in Barrett's esophagus," *Gastroenterology* **111**, 93–101 (1996).
11. J. M. Poneros, S. Brand, B. E. Bouma, G. J. Tearney, C. C. Compton, and N. S. Nishioka, "Diagnosis of specialized intestinal metaplasia by optical coherence tomography," *Gastroenterology* **120**(1), 7–12 (2001).
12. M. Anidjar, O. Cussenot, S. Avrillar, D. Ettori, P. Teillac, and P. Le Duc, "The role of laser-induced autofluorescence spectroscopy in bladder tumor detection," *Ann. N.Y. Acad. Sci.* **838**, 130–142 (1998).
13. A. S. Haka, K. E. Shafer-Peltier, M. Fitzmaurice, J. Crowe, R. R. Dasari, and M. S. Feld, "Diagnosing breast cancer by using Raman spectroscopy," *Proc. Natl. Acad. Sci. U.S.A.* **102**(35), 12371–12376 (2005).
14. T. M. Breslin, F. Xu, G. M. Palmer, C. Zhu, K. W. Gilchrist, and N. Ramanujam, "Autofluorescence and diffuse reflectance properties of malignant and benign breast tissues," *Ann. Surg. Oncol.* **11**(1), 65–70 (2004).
15. D. Hanahan and R. A. Wienberg, "The hallmarks of cancer," *Cell* **100**(1), 57–70 (2000).
16. S. Lowe, E. Cepero, and G. Evan, "Intrinsic tumour suppression," *Nature (London)* **432**, 307–315 (2004).
17. R. Gerl and D. L. Vaux, "Apoptosis in the development and treatment of cancer," *Carcinogenesis* **26**(2), 263–270 (2005).
18. M. Brewer, et al., "Fluorescence spectroscopy as a biomarker in a cell culture and in a nonhuman primate model for ovarian cancer chemopreventive agents," *J. Biomed. Opt.* **7**(1), 20–26 (2002).

19. L. Morbidelli, M. Monici, N. Marziliano, A. Cogoli, F. Fusi, J. Waltenberger, and M. Ziche, "Simulated hypogravity impairs the angiogenic response of endothelium by up-regulating apoptotic signals," *Biochem. Biophys. Res. Commun.* **334**(2), 491–499 (2005).
20. P. X. Petit, M. C. Gendron, N. Schrantz, D. Metivier, G. Kroemer, Z. Maciorowska, F. Sureau, and S. Koester, "Oxidation of pyridine nucleotides during Fas- and ceramide-induced apoptosis in Jurkat cells: correlation with changes in mitochondria, glutathione depletion, intracellular acidification and caspase 3 activation," *Biochem. J.* **353** (2), 357–367 (2001).
21. M. Poot and R. H. Pierce, "Detection of changes in mitochondrial function during apoptosis by simultaneous staining with multiple fluorescent dyes and correlated multiparameter flow cytometry," *Cytometry* **35** (4), 311–317 (1999).
22. F. Wolbers, H. Andersson, A. van den Berg, and I. Vernes, "Apoptosis induced kinetic changes in autofluorescence of cultured HL60 cell-possible application for single cell analysis on chip," *Apoptosis* **9**, 749–755 (2004).
23. L. Michea, C. Combs, P. Andrews, N. Dimitrieva, and M. B. Burg, "Mitochondrial dysfunction is an early event in high-NaCl-induced apoptosis of mIMCD3 cells," *Am. J. Physiol. Renal Physiol.* **282** (6), F981–F990 (2002).
24. A. Shino, M. Haida, B. Beauvoit, and B. Chance, "Three-dimensional redox image of the normal gerbil brain," *Neuroscience* **91**, 1581–1585 (1999).
25. Z. Zhang, D. Blessington, H. Li, T. M. Busch, J. Glickson, Q. Luo, B. Chance, and G. Zheng, "Redox ratio of mitochondria as an indicator for the response of photodynamic therapy," *J. Biomed. Opt.* **9** (4), 772–778 (2004).
26. J. C. Haselgrove, C. L. Bashford, C. H. Barlow, B. Quistorff, B. Chance, and A. Mayevsky, "Time resolved 3-dimensional recording of redox ratio during spreading depression in gerbil brain," *Brain Res.* **506** (1), 109–114 (1990).
27. H. D. Vishwasrao, A. A. Heikal, K. A. Kasischke, and W. W. Webb, "Conformational dependence of intracellular NADH on metabolic state revealed by associated fluorescence anisotropy," *J. Biol. Chem.* **280**(26), 25119–25126 (2005).
28. D. E. Harrison and B. Chance, "Fluorimetric technique for monitoring changes in the level of reduced nicotinamide nucleotides in continuous cultures of microorganisms," *Appl. Microbiol.* **19**(3), 446–450 (1970).
29. D. L. Jones, R. M. Alani, and K. Münger, "The human papillomavirus E7 oncoprotein can uncouple cellular differentiation and proliferation in human keratinocytes by abrogating $p21^{Cip1}$-mediated inhibition of cdk2," *Genes Dev.* **11**, 2101–2111 (1997).
30. J. V. Rocheleau, W. S. Head, and D. W. Piston, "Quantitative NAD(P)H/flavoprotein autofluorescence imaging reveals metabolic mechanisms of pancreatic islet pyruvate response," *J. Biol. Chem.* **279**(30), 31780–31787 (2004).
31. S. Brandt, *Data Analysis: Statistical and Computational Methods for Scientists and Engineers*, 3rd ed., pp. xxxii 652, Springer, New York (1999).
32. G. R. Norman and D. L. Streiner, *Biostatistics: The Bare Essentials*, 2nd ed., pp. x, 324, B.C. Dekker, Hamilton (2000).
33. M. J. Mate, et al., "The crystal structure of the mouse apoptosis-inducing factor AIF," *Nat. Struct. Mol. Biol.* **9**(6), 442–446 (2002).
34. S. A. Susin, et al., "Molecular characterization of mitochondrial apoptosis-inducing factor," *Nature (London)* **397**, (6718), 441–446 (1999).
35. H. Ye, et al., "DNA binding is required for the apoptogenic action of apoptosisinducing factor," *Nat. Struct. Mol. Biol.* **9**(9), 680–684 (2002).
36. E. Daugas, et al., "Mitochondrio-nuclear translocation of AIF in apoptosis and necrosis," *FASEB J.* **14**(5), 729–739 (2000).
37. S. A. Susin, et al., "Two distinct pathways leading to nuclear apoptosis," *J. Exp. Med.* **192**(4), 571–580 (2000).
38. K. D'Herde, B. De Prest, S. Mussche, P. Schotte, R. Beyaert, R. Van Coster, and F. Roels, "Ultrastructural localization of cytochrome c in apoptosis demonstrates mitochondrial heterogeneity," *Cell Death Differ* **7**, 331–337 (2000).
39. T. Collins, M. Berridge, P. Lipp, and M. Bootman, "Mitochondria are morphologically and functionally heterogeneous within cells," *EMBO J.* **21**, 1616–1627 (2002).
40. A. V. Kuznetsov, Y. Usson, X. Leverve, and R. Margreiter, "Subcellular heterogeneity of mitochondrial function and dysfunction: evidence obtained by confocal imaging," *Mol. Cell. Biochem.* **256–257**(1–2), 359–365 (2004).
41. J. V. Rocheleau, W. S. Head, W. E. Nicholson, A. C. Powers, and D. W. Piston, "Pancreatic islet beta-cells transiently metabolize pyruvate," *J. Biol. Chem.* **277**(34), 30914–30920 (2002).
42. Z. Shiffer, N. Zurgil, Y. Shafran, and M. Deutsch, "Analysis of laser scattering pattern as an early measure of apoptosis," *Biochem. Biophys. Res. Commun.* **289**(5), 1320–1327 (2001).
43. N. N. Boustany, R. Drezek, and N. V. Thakor, "Calcium-induced alterations in mitochondrial morphology quantified in situ with optical scatter imaging," *Biophys. J.* **83**(3), 1691–1700 (2002).